# Investigation of Mesh Regularization in MAT_224 for Subsequent Use in Impact Simulations

Troy Lyons
Kiran D'Souza
*Gas Turbine Laboratory at The Ohio State University*

## Abstract

*This work is focused on the use of mesh regularization, which is an attempt to remove the mesh dependence from finite element simulations. Mesh regularization techniques are often used to help match experimental data and allow for reduced computational cost. The MAT_224 material model within LS-DYNA® allows users to define a failure criterion that is dependent on temperature, strain rate, stress state, and element size. The element size dependence in the failure criterion can help reduce the influence of mesh size on simulated results under certain circumstances. However, some issues may arise when the MAT_224 material model is applied to different geometries, stress states, and element sizes than the regularization curve was originally created from. In this work, the conditions to best use mesh regularization are investigated, which is done with various comparisons using experimental and simulated data, both with and without mesh regularization.*

## Introduction

Finite element results often have some dependence on the meshes used in their models. Typically, this dependence decreases with mesh refinement, however this is not always the case [1]. The dependence results have on a mesh is undesirable, since it is purely numerical and not an artifact of any physical phenomenon. Analysts often look to a variety of techniques to reduce or "regularize" the dependence that the results have on the finite element mesh. This is commonly referred to as mesh regularization.

One common mesh regularization approach is to average the damage/failure criteria of surrounding elements for each given element. This averaging can mitigate strain localization in a given element where such localization may not be physical. This approach was written in [2] and can be used within LS-DYNA via MAT_NONLOCAL [3]. An example of MAT_NONLOCAL in use was written by [4] for the analysis of the ballistic perforation of aluminum plates.

Another common mesh regularization approach, which is the focus of this work, is to alter the element failure criterion based upon element size. Several material models in LS-DYNA offer this capability including MAT_TABULATED_JOHNSON_COOK (MAT_224), MAT_224_GYS, MAT_264. MAT_ADD_EROSION allows users to add a failure criterion to any material model with an optional regularization technique of this type. This can be attractive to analysts, since if they are able to get the same result with a coarse mesh as a refined mesh, they could reduce computational cost by using the coarse mesh. There are several examples of this approach to regularization being used successfully to reduce mesh dependence. A few examples include the bolted connection modeling by Hadjioannou et. al. [5], and modeling of tensile experiments by Haight et. al. [6].

Despite its potential advantages, mesh regularization (especially regularization by scaling the failure criterion) must be used with some care to avoid "over fitting" a finite element model to some particular simulation or set of parameters. It is possible that using a mesh regularization technique to fit the results under one set of conditions would be at the cost of diminishing accuracy under different conditions (perhaps other geometries, stress states, element types and sizes, etc.). MAT_224, among other material models, attempts to alleviate this issue. It has an option to define a mesh regularization in its failure criterion that can also be dependent on the stress state in addition to element size.

The element failure criterion, *F*, for MAT_224, is the time integrated ratio of the plastic strain rate $\dot{\varepsilon_p}$, to the plastic failure strain under the conditions of each timestep $\varepsilon_{pf}$.

$$F = \int \frac{\dot{\varepsilon}_{\mathrm{p}}}{\varepsilon_{\mathrm{pf}}} dt$$

The plastic failure strain of MAT_224 resembles the original Johnson-Cook model [7], where the plastic failure strain is the product of several simpler functions:

$$\varepsilon_{pf} = f(\tau, \theta_L) g(\dot{\epsilon_p}) h(T) i(l_c, \tau, \theta_L)$$

Tabulated functions *f, g, h*, and *i* are defined by the user, and are functions of the plastic strain rate $\dot{\varepsilon_p}$, temperature, *T,* element size $l_c$, stress triaxiality $\tau$, and Lode parameter $\theta_L$. The triaxiality and Lode parameters are functions of the invariants of the stress tensor, for more information see [8,9].

For use in studies involving fan blade out and foreign object ingestion, the Federal Aviation Administration (FAA) has been working to develop a MAT_224 material model for the titanium alloy Ti-6Al-4V. That material model is publicly available on the LS-DYNA Aerospace Working Group (AWG) website [10]. That AWG model comes with a mesh regularization curve for elements ranging from 0.1 to 0.4 mm in size (there are extra/dummy data points at 0.0 and 0.5 mm to prevent serious inaccuracies from extrapolating the curve).

The regularization curve of the AWG Ti-6Al-4V model created by Haight et. al. [6] motivated this work. In their unmanned aerial vehicle (UAV) ingestion study, Lyons and D'Souza [11] used the AWG Ti-6Al-4V MAT_224 model to simulate potential damage to a solid titanium fan if it were to ingest a UAV. Fan blades of a jet engine are several orders of magnitude larger than that of the tensile specimen used to create the AWG Ti-6Al-4V material model's regularization curve. Elements in the range of 0.1 to 0.4 mm, which are reasonable for a tensile specimen, will result in meshes that are dense and prohibitively expensive on larger structures such as fan blades.

Lyons and D'Souza [11] chose to use the mesh regularization value at the largest element size from the AWG model by Haight et. al. [6]. This type of decision prompted this investigation to determine what approach should be taken in future engine ingestion impact studies for mesh regularization. This work looks to consider potential options such as extending the existing mesh regularization curve or using the AWG model but without mesh regularization. This is accomplished by looking at the effectiveness of mesh regularization (via scaling the failure criterion) by comparing simulations with different geometries, and meshes, with and without regularization.

The simulations presented herein are of quasi-static uniaxial tension experiments. These are the same type of experiments that were simulated to create the mesh regularization curve in the AWG titanium model [6]. The experiment being simulated in this work is the slowest strain rate ($10^{-4}$ per second) of the uniaxial tension tests of Ti-6Al-4V from 0.5-inch-thick plates conducted by Hammer [12]. This is a different strain rate than what was used by Haight et. al. ($10^{-2}$ per second) to create the regularization curve [6]. This ensures the validity of the quasi-static assumption in this work, although the strain rate used by Haight et. al. is also sufficient. Any difference is not an issue, since the trends will be the same and this work focuses on how regularization affects the displacement to failure for a given experiment.

## Methodology

This section will first give the tensile specimen geometries and boundary conditions. Next, the key parameters used in the LS-DYNA simulations will be given. This includes both key settings in the input file and information

on how the data was extracted. After that, details specific to how the simulations of quasi-static experiments are given, including changes necessary to the AWG Ti-6Al-4V model, and the determination of a loading rate that is sufficiently slow to avoid any artificial dynamic effects. Finally, a comparison to experimental data is made to validate the approach used in this work.

The dimensions for the geometry of the full tensile specimen simulated in this work, is called the "thin smooth specimen" in the plane stress fracture testing series by Hammer [12]. The portions of the tensile specimen far removed from the gage portion are omitted to reduce computational cost, as done by Haight et. al. [6].

Explicit time integration of quasi-static experiments can be computationally expensive due to the large amount of time being simulated. To reduce the model size, symmetry of the tensile specimen geometry can be used to create a 1/8 model that yield results that match the full model. The 1/8 model can be seen in Fig. 1. The symmetry planes were defined with BOUNDARY_SPC_SYMMETRY_PLANE, which restricts nodes along each symmetry plane from having any motion normal to that plane. A comparison of the 1/8 model to the full model was made and they agreed well, as is presented in the Appendix.

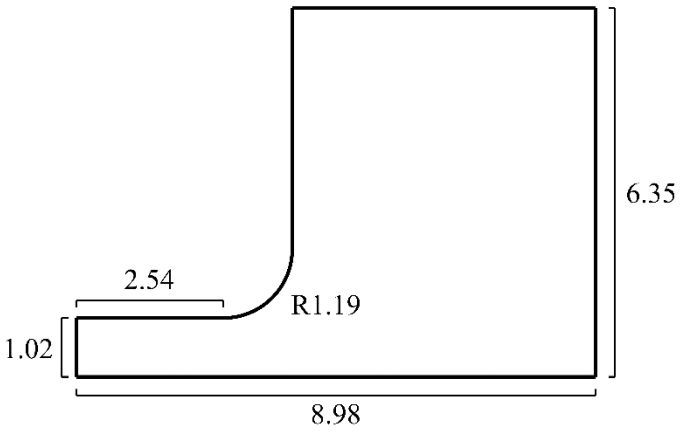


a) The 1/8 symmetry geometry. All dimensions are in millimeters. The full tensile specimen is 0.762 mm thick, and the symmetry tensile specimen is 0.381 mm thick.

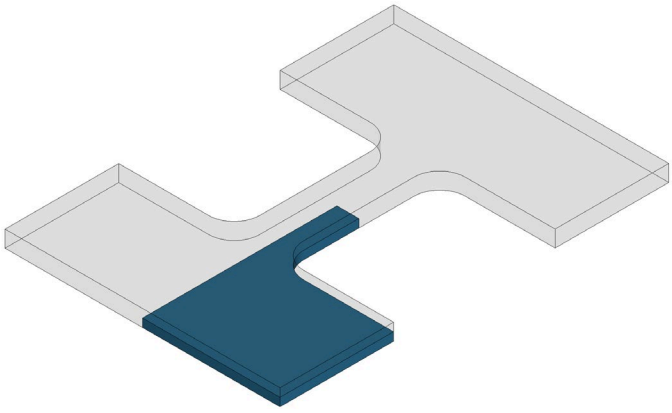

b) The 1/8 symmetry geometry (blue) overlaid with the full tensile specimen geometry (partially transparent grey)

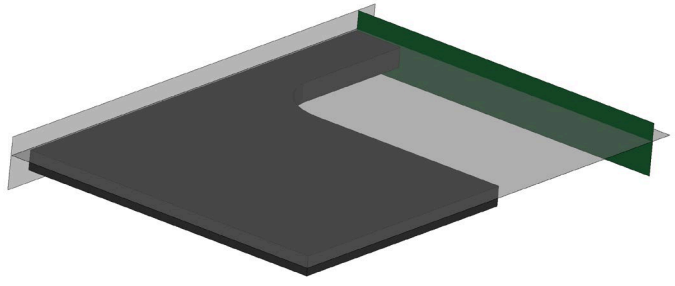

c) The symmetry geometry with its planes of symmetry. The plane shown in green is only a symmetry plane for quasi-static loading rates, the other two (partially transparent grey) are symmetry planes regardless of the loading rate.

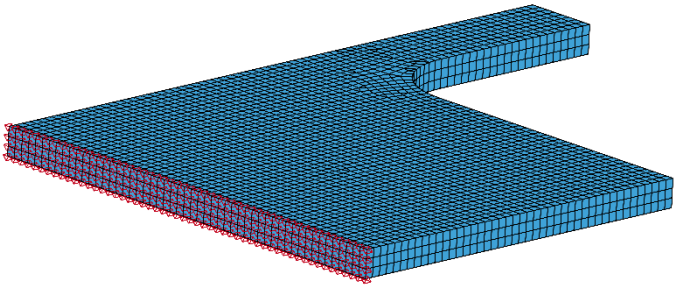

d) The nodes on the end face (highlighted in red) form a nodal rigid body, and their motion is prescribed at constant velocity to cause the deformation

Figure 1: The geometry and symmetry planes for the tension simulations

In this work, several simulations use a geometry that is 10 times larger in every spatial direction as the geometry shown in Fig. 1. This will allow for the investigation of several aspects of mesh regularization with a different geometry than what was used to create the regularization curve in the AWG Ti-6Al-4V MAT_224 model, while still keeping the stress state the same. The gage length, width, and thickness of the 10x scaled (but still also a 1/8 symmetry model analogous to Fig. 1a) geometry was 25.4, 10.2, and 3.81 mm respectively.

The approach used to create the 10x scaled (large) geometry was to mesh the unscaled, relatively small geometry shown in Fig. 1, and scale up those meshes by a factor of 10 in all directions. Table 1 has the sizes of the elements in the gage portion of the tensile specimen for both geometries. As described in this work, the mesh label, as given in Table 1 (e.g., SM0.4LG4.0), and geometry (unscaled vs. 10x scaled), both are necessary to determine the element size in any particular simulation.

Table 1: The sizes of elements in the gage portion of the tensile specimen for each mesh in the unscaled (small) and 10x scaled (large) geometries.

| Mesh Label | Unscaled Geometry Element Size (mm) | 10x Scaled Element Size (mm) |
|---|---|---|
| SM0.4LG4.0 | 0.338 | 3.38 |
| SM0.2LG2.0 | 0.19 | 1.9 |
| SM0.16LG1.6 | 0.159 | 1.59 |
| SM0.12LG1.2 | 0.121 | 1.21 |
| SM0.08LG0.8 | 0.0762 | 0.762 |
| SM0.04LG0.4 | 0.0381 | 0.381 |
| SM0.02LG0.2 | 0.02 | 0.2 |

The mesh labels were defined in such a way to quickly give the "target" (what was entered into Hypermesh, but many element sizes are not exactly possible since each segment can only have an integer number of nodes along it) mesh size for both the unscaled (small) and 10x scaled (large) geometry. Each mesh label is of the form:

SM[*size1*]LG[*size2*]

*size1:* The target/approximate mesh size for the unscaled (small) geometry
*size2:* The target/approximate mesh size for the 10x scaled (large) geometry

Knowledge of the geometry (unscaled vs 10x scaled) and the mesh label remove any ambiguity in which meshes are being compared.

Discussed next are the details of the parameters used for the input into LS-DYNA and methods of data extraction. All simulations were run with LS-DYNA version 10.1 using MPP parallelization and double precision. The nodes along the face highlighted in Fig. 1d were defined to be a nodal rigid body via CONSTRAINED_NODAL_RIGID_BODY_SPC. Only the translational degree of freedom for that rigid body along the direction of the length of the gage section was left active.

All simulations used single point integration solid elements (ELFORM=1 under SECTION_SOLID). The gage section of each tensile specimen was made of purely hexahedral elements, and the remainder of the tensile

specimen, where strains were far smaller, was meshed with a hexahedral dominant mesh, having less than 1% pentahedrons. ESORT was set to two under CONTROL_SOLID for proper treatment of those elements.

There were several key parameters in the control cards. To prevent hourglass instability, Flanagan-Belytschko [13] hourglass control (IQH=4, QH=0.03 under CONTOROL_HOURGLASS) was used. No mass scaling was used in any of the simulations. Hourglass, stonewall, sliding, and damping energies were all tracked under CONTROL_ENERGY. Due to the quasi-static nature of these simulations, some key LS-DYNA defaults were permissible that would not typically be used in impact simulations. These include neglecting second order objective stress update (OSU=0 under CONTROL_ACCURACY) and using the default 0.9 for the time step scale factor under CONTROL_TIMESTEP. Simulations to verify each of those settings was run, and no significant changes to results were observed.

Forces and displacements are calculated from SECFORC and NODOUT output, respectively. Forces and positions were extracted at 1000 evenly spaced time intervals throughout every simulation. A set of nodes (highlighted in blue in Fig. 2a) and elements (highlighted in red in Fig. 2b) near the end of the gage section were defined and referenced in DATABASE_CROSS_SECTION_SET to serve as a reference location where the forces were being calculated. The component of force along the direction of the gage length is multiplied by four before being reported to capture the force of the full tensile specimen geometry. The spatial coordinates of a node (highlighted in green in Fig. 2a) were extracted from DATABASE_HISTORY_NODE_SET. The component of position for the node along the length of the gage is doubled to represent the length in the full tensile specimen geometry.

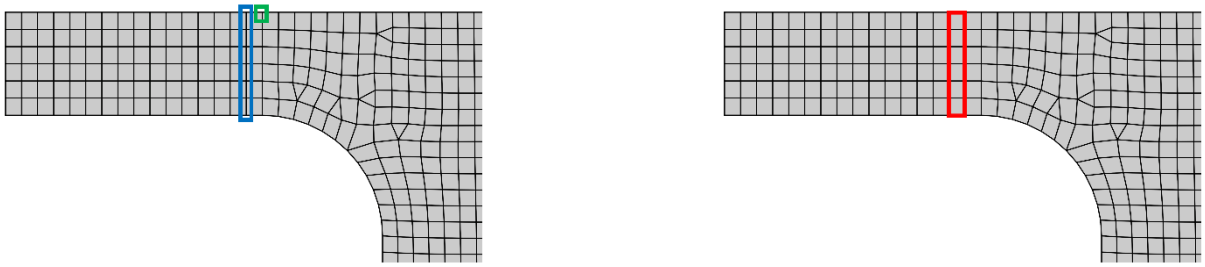

a) Nodes to measure force (blue) and displacement (green)

b) Elements to measure force

Figure 2: The nodes and elements used to measure force and displacement of the gage portion of the tensile specimen

There are also a few aspects of the finite element modeling that are specific to modeling quasi-static experiments. The Ti-6Al-4V titanium material model [6] available on the LS-DYNA AWG website [10] is primarily intended for short-duration impact simulations. That model is strain rate dependent. Since these simulations are explicitly integrated in time, loading must be applied artificially faster than they would be in the actual quasi-static experiment for the simulation to be computationally tractable. For results to match, this requires the effective stress vs effective plastic strain curve made from the quasi-static strain rate is used. The second aspect of modeling the quasi-static experiments is to determine a loading rate that is fast enough to avoid excessive computational cost, but sufficiently slow so results are not altered. This task will be discussed after going through the changes to the Ti-6Al-4V titanium material model available on the LS-DYNA AWG website [10].

To prepare the AWG Ti-6Al-4V titanium material model for use in the quasi-static tests, the thermal dependence must be removed and the stress-strain relation at the proper strain rate must be selected. The AWG Ti-6Al-4V MAT_224 model comes with a thermal dependence to model the localized heating that occurs from plastic deformation. Under many impact conditions, deformation occurs so quickly that heat generated from plasticity

will have little time to conduct to nearby areas. Thus, impact simulations are typically approximated as adiabatic. Quasi-static experiments have the opposite extreme, where they occur over such long time periods that heat generated through plasticity has sufficient time to conduct throughout the entire structure. For this reason, quasi-static experiments are approximated as isothermal.

To properly match the thermal conditions of a quasi-static tension test, the thermal dependence of the flow stress and that failure criterion were removed. Following [14], this was done by removing the referenced table LCKT and load curve LCH in MAT_224, respectively. This way elements can still have temperature increases from plastic deformation, but this does not alter the constitutive relation.

In the AWG Ti-6Al-4V MAT_224 material model, the flow stress is also dependent on the strain rate in addition to the stress state and temperature. Since these simulations will be using an artificially large loading rate, care must be taken to ensure that the quasi-static flow stress and failure criterion reflect that of a quasi-static test. To do this, TABK1 under MAT_224 was switched to only reference the curve relating flow stress and plastic strain associated with the slowest strain rate in the AWG model. The curve referenced in LCG (under MAT_224) was removed to prevent any influence the artificial strain rate would have on the failure criterion. The last modification to the AWG model was to remove the mesh regularization (LCI) except where otherwise noted in this paper.

The artificial loading rate must not introduce vibrations that would be non-existent in the real-life quasi-static tension experiment. The artificially high loading rate of the simulation should be sufficiently small such that any further reduction in the loading rate of the simulation does not significantly affect results. The nodes highlighted in red of Fig. 1d move with a constant prescribed velocity parallel to the gage length direction. In this work, a value for the displacement of that nodal rigid body was chosen such that all the meshes would have modeled failure by the time of reaching that displacement. Different values for the final displacement were used for the unscaled and 10x scaled geometry. The displacement of the nodal rigid body at the end of the simulation, was 1.4 mm for the full tensile specimen (0.7 mm for the symmetry model) for the unscaled geometry and 14 mm (7.0 for the symmetry model) for the 10x scaled geometry. The prescribed velocity of the nodes highlighted in Fig. 1d was constant. The sufficiently long duration was found to be 5 ms (see Fig. 3a) for the unscaled geometry and 50 ms for the 10x scaled geometry (see Fig 3b).

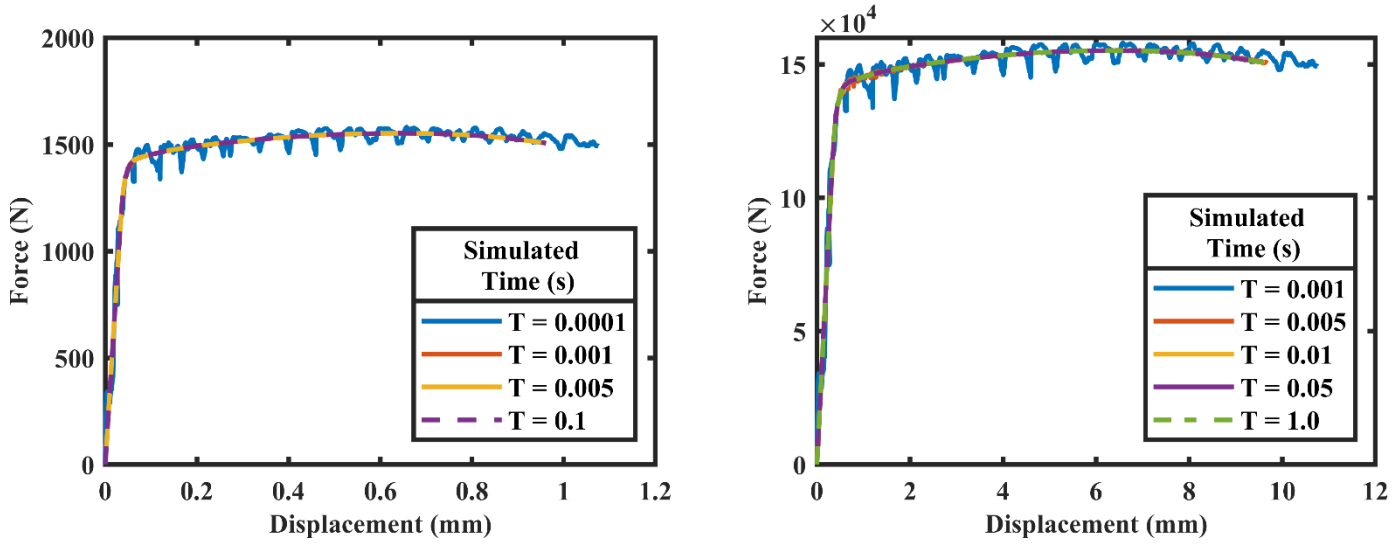


a) Unscaled (small) geometry

b) 10x scaled (large) geometry

Figure 3: Determination of the artificial loading rate via simulation duration for the a) unscaled and b) 10x scaled geometries. The mesh labeled SM0.12LG1.2 in Table 1 was used for both geometries.

The last remaining task is to validate the simulations used in this work. The experiment modeled in this work was done by Hammer [12]. A load cell and extensometer were used to measure the force and deformation of the tensile specimen, respectively. Hammer reports the logarithmic/true stress σ and logarithmic/true strain ε, which can be related to the engineering stress $\sigma_e$, and engineering strain $\epsilon_e$, gage length $l$, and initial gage length $l_0$:

$$\varepsilon_e = \frac{l - l_0}{l_0}$$

Derivations of these formulas can be found in several literature sources, including [6].

$$\varepsilon = ln(\varepsilon_e + 1)$$

To get the stresses, we also need the cross-sectional force, $f$, and initial cross-sectional area, $A_0$:

$$\sigma_e = \frac{f}{A_0}$$

This gives the logarithmic/true stress, $\sigma$:

$$\sigma = \sigma_e(1 + \varepsilon_e)$$

Fig. 4 shows that the simulated results are in good agreement with the experimental results from Hammer [12].

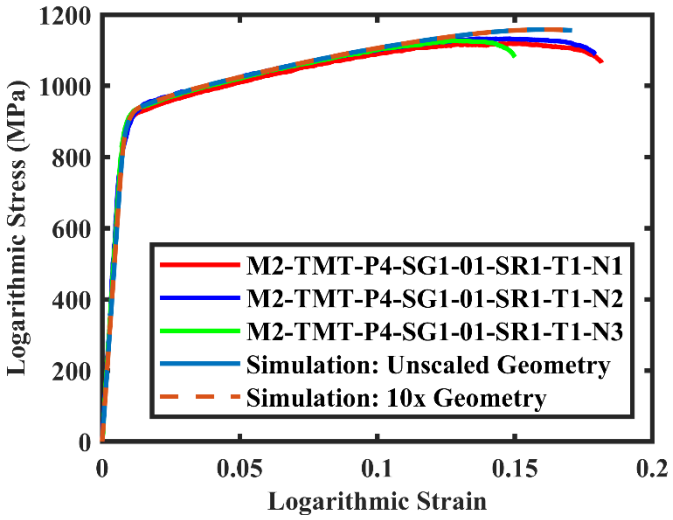


Figure 4: Comparison to experiment [12] using the most refined mesh, SM0.02LG0.2

## Results: Mesh Refinement Study at Multiple Geometric Scales with and without Mesh Regularization

Simulations of quasi-static, uniaxial tension tests at different geometric scales are used to look at convergence under refinement both with and without mesh regularization. The use of multiple geometric scales will provide insight into the effectiveness of mesh regularization for elements of similar size. The stress state will remain uniaxial tension, but the geometry will be different. First, the unscaled (small) geometry will be investigated, and

then the 10x (large) geometry. The key parameters for these simulations are described in the Methodology section of this work, as well as the explanation of the mesh labeling convention.

All of the meshes for the unscaled (small) geometry have their element sizes described in the middle columns of Table 1 and Table 2. The displacement to failure for each mesh, without the use of mesh regularization, is given in Table 2.

Table 2: The displacement to failure for each mesh of the unscaled (small) geometry without the use of mesh regularization

| Mesh Label | Unscaled Geometry Element Size (mm) | Displacement to Failure (mm) |
|---|---|---|
| SM0.4LG4.0 | 0.338 | 1.08 |
| SM0.2LG2.0 | 0.19 | 0.981 |
| SM0.16LG1.6 | 0.159 | 0.97 |
| SM0.12LG1.2 | 0.121 | 0.96 |
| SM0.08LG0.8 | 0.0762 | 0.952 |
| SM0.04LG0.4 | 0.0381 | 0.946 |
| SM0.02LG0.2 | 0.02 | 0.946 |

Table 2 shows clear convergence with mesh refinement. The resulting force vs. displacement curve corresponding to a *full* (instead of what was simulated directly from the symmetry version) geometry are given in Fig. 5a, and in Fig. 5b this result is zoomed in near failure. The displacement to failure approaches the most refined result, SM0.02LG0.2 monotonically with mesh refinement.

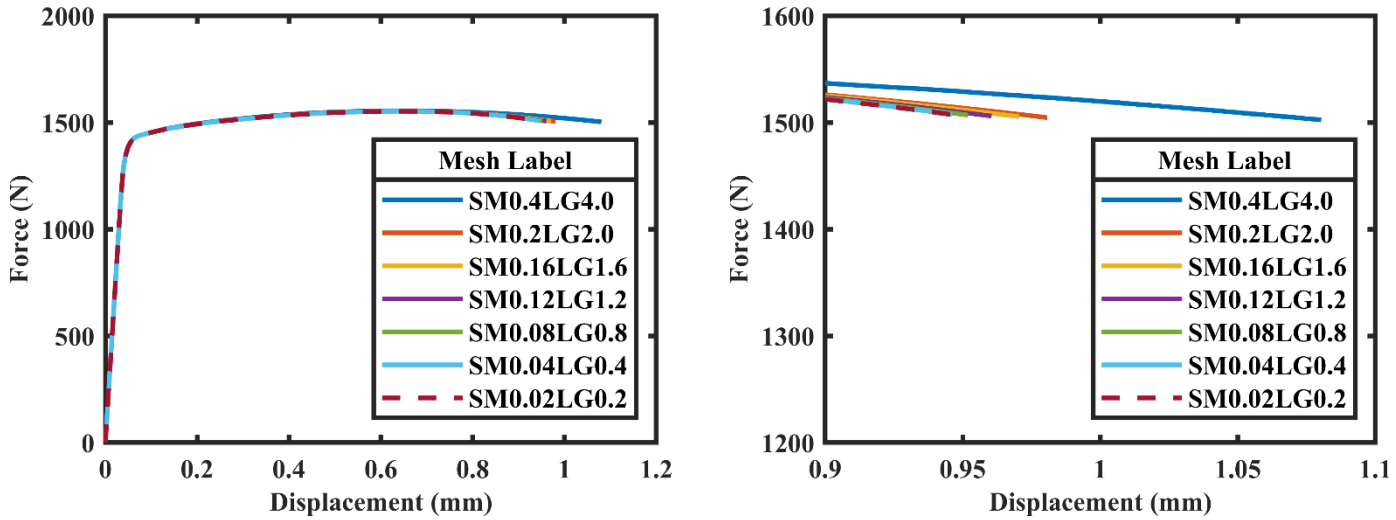


a) Mesh refinement without regularization, unscaled geometry

b) Zoomed in on the failure portion of the curves shown in part a)

Figure 5: Refinement study using all the meshes for the unscaled geometry, without mesh regularization

Next, simulations analogous to those of Table 2 and Fig. 5 were run while invoking the AWG mesh regularization. For these the unscaled (small) geometry was still being used. Only meshes with element sizes falling within the AWG mesh regularization curve (0.1 to 0.4 mm) were used to avoid any extrapolation of that curve. Results of these simulations are given in Table 3.

| Table 3: The displacement to failure for each mesh of the unscaled (small) geometry with the use of the AWG mesh regularization curve | | |
|---|---|---|
| Mesh Label | Unscaled Geometry Element Size (mm) | Displacement to Failure (mm) |
| SM0.4LG4.0 | 0.338 | 1.041 |
| SM0.2LG2.0 | 0.19 | 0.983 |
| SM0.16LG1.6 | 0.159 | 0.977 |
| SM0.12LG1.2 | 0.121 | 0.972 |

The AWG mesh regularization curve used to generate the results shown in Table 3 and Fig. 6 was created by Haight et. al [6]. Haight's intended purpose was to get results to best match their baseline mesh, which had 0.2 mm sized elements. The results in their work have tighter agreement than those presented here. The regularization used for the unscaled geometry as shown in Table 3 and Fig. 6 brings the meshes closer to the result of SM0.2LG2.0 (approximately 0.2 mm elements) than the unregularized results shown in Table 2 and Fig. 5, meaning the trend is consistent with Haight et. al [6]. Choices of element type, hourglass, and stress-strain curve used in this work are different than what was used in [6]. These choices give slight differences to the results here. However, the trends are the same and the regularization improves agreement for the unscaled geometry simulations as it would in [6].

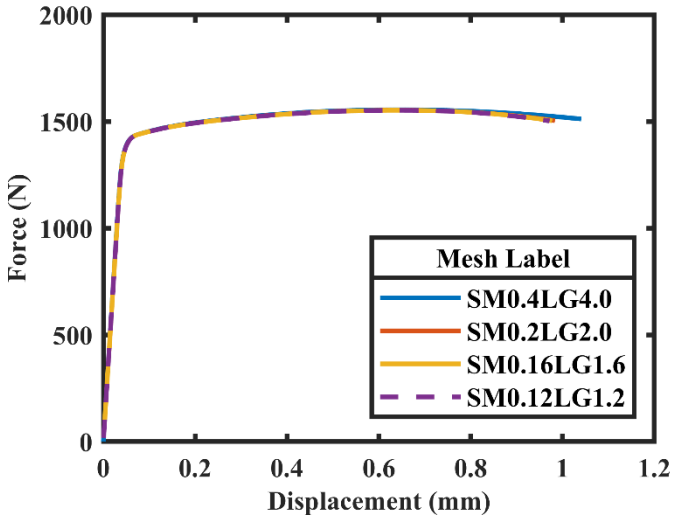


a) Refinement AWG reg, unscaled geometry

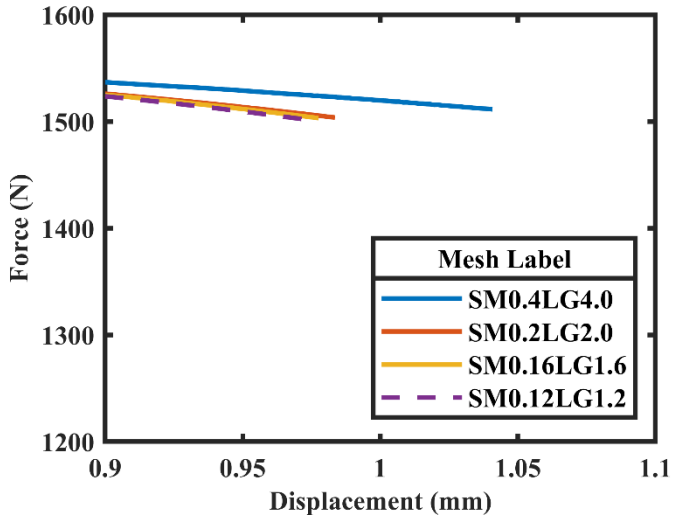


b) Zoomed in on the failure portion of the curves shown in part a)

Figure 6: Refinement study using the meshes with elements within the range of 0.1 to 0.4 mm on the unscaled geometry with AWG mesh regularization.

The agreement meshes have to the SM0.2LG2.0 (approx. 0.2 mm element size) result is given in Table 4. In Table 4, results without regularization are being compared (via percent difference) to the SM0.2LG2.0 result also without regularization, likewise results with regularization are given the percent difference from the SM0.2LG2.0 result also with regularization. Some of the meshes were not simulated with regularization due to the element sizes falling outside of the AWG regularization curve [6]. The percentage differences show that mesh regularization (on the unscaled geometry) is successful in improving agreement to the SM0.2LG2.0 (approx. 0.2 mm element size) results, as it was intended to do [6].

| Table 4: The percent difference in the displacement to failure for each mesh of the unscaled (small) geometry. These values compare simulations without regularization to the SM0.2LG2.0 (approx. 0.2 mm mesh) result also without regularization. Likewise, simulations with AWG regularization compare to SM0.2LG2.0 (approx. 0.2 mm mesh) result also with AWG regularization. | | |
|---|---|---|
| Mesh Label | % Difference in Displacement from Failure of SM0.2LG2.0 (0.981 mm) without regularization | % Difference in Displacement to Failure from SM0.2LG2.0 (0.983 mm) with AWG regularization |
| SM0.4LG4.0 | 10.1 | 5.9 |
| SM0.2LG2.0 | - | - |
| SM0.16LG1.6 | -1.12 | -0.61 |
| SM0.12LG1.2 | -2.14 | -1.12 |
| SM0.08LG0.8 | -2.96 | n/a |
| SM0.04LG0.4 | -3.57 | n/a |
| SM0.02LG0.2 | -3.57 | n/a |

Next, simulations analogous to those in Fig. 5, 6 and Tables 2-4 were run on the 10x scaled (large) geometry. This tests how well the mesh regularization via scaling the failure criterion works on a different geometry than the one used to create the regularization curve. As shown in Table 1, element sizes in the gage section are quite similar for the SM0.02LG0.2 and SM0.04LG0.4 meshes for the 10x scaled (large) geometry as the SM0.2LG2.0 and SM0.4LG4.0 meshes in the unscaled (small) geometry. The stress state is essentially the same, quasi-static, uniaxial tension, as the previous results shown in Fig. 5, 6 and Tables 2-4.

| Table 5: The displacement to failure for each mesh of the 10x scaled (large) geometry without the use of mesh regularization | | | |
|---|---|---|---|
| Mesh Label | 10x Scaled Geometry Element Size (mm) | Displacement to Failure (mm) | % Difference from SM0.02LG0.2 |
| SM0.4LG4.0 | 3.38 | 10.8 | 14.2 |
| SM0.2LG2.0 | 1.9 | 9.81 | 3.7 |
| SM0.16LG1.6 | 1.59 | 9.704 | 2.6 |
| SM0.12LG1.2 | 1.21 | 9.605 | 1.5 |
| SM0.08LG0.8 | 0.762 | 9.519 | 0.6 |
| SM0.04LG0.4 | 0.381 | 9.48 | 0.2 |
| SM0.02LG0.2 | 0.2 | 9.46 | - |

Table 5 provides results for the 10x scaled (large) geometry simulations without mesh regularization. Just like the analogous simulations using the unscaled (small) geometry, the displacement to failure converges with mesh refinement. As expected, the displacement to failure of 10x scaled geometry without regularization results are 10 times the displacement to failure of the same meshes in the unscaled geometry. The slight exception

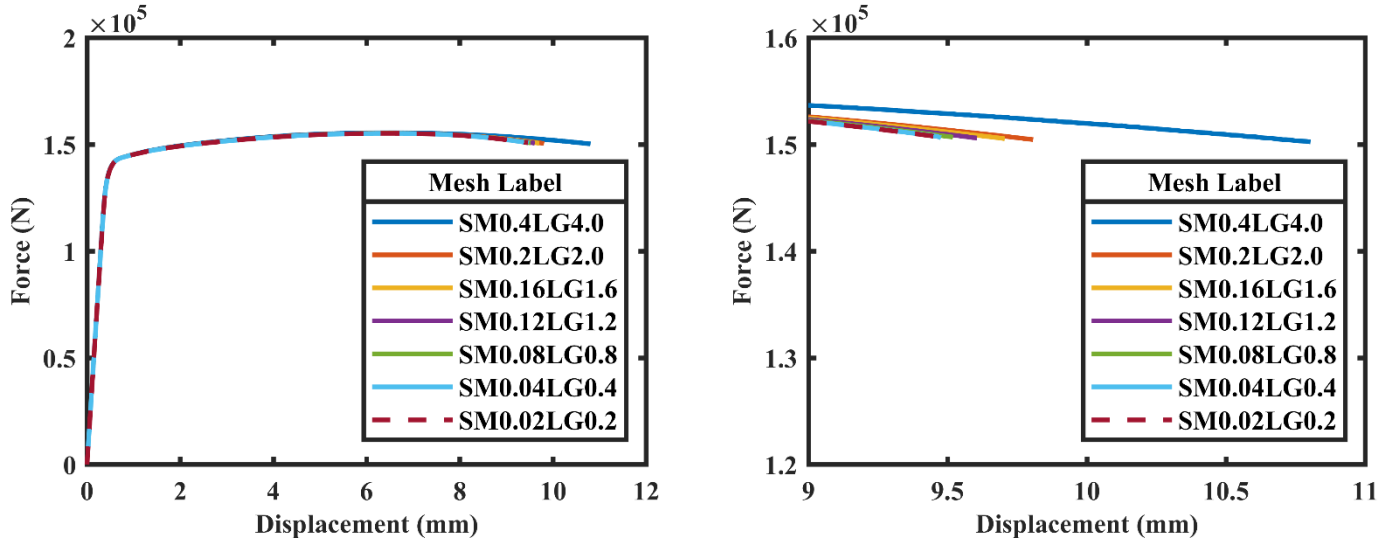


a) Mesh refinement without regularization, 10x scaled geometry

b) Zoomed in on the failure portion of the curves shown in part a)

Figure 7: Refinement study using all the meshes for the 10x scaled geometry without mesh regularization

is the SM0.04LG0.4 result. Although a somewhat large (1000) number of force and displacement data points were collected, the SM0.04LG0.4 10x scale result had failure occur at one data point before the unscaled result. This difference is sufficient for the small discrepancy between the unscaled and 10x scaled results. Plots of the stress-strain and zoomed stress strain curves for the 10x scaled (large) geometry without mesh regularization are shown in Fig. 7.

Table 6: The displacement to failure for each mesh of the 10x scaled (large) geometry with the use of the AWG mesh regularization curve

| Mesh Label | 10x Scaled Geometry Element Size (mm) | Displacement to Failure (mm) | % Difference from SM0.02LG0.2 |
|---|---|---|---|
| SM0.04LG0.4 | 0.381 | 9.18 | -2.96 |
| SM0.02LG0.2 | 0.2 | 9.46 | - |

Results from simulations with the 10x scaled (large) geometry using the AWG regularization are included in Table 6. Only the two meshes having element sizes falling within the range of the regularization curve were simulated. The force and displacement plots for these simulations are given in Fig. 8. Mesh regularization introduces a scale dependence to the material model, which causes the displacements to failure in Table 6 to not be 10 times those found in the analogous unscaled geometry results of Table 3.

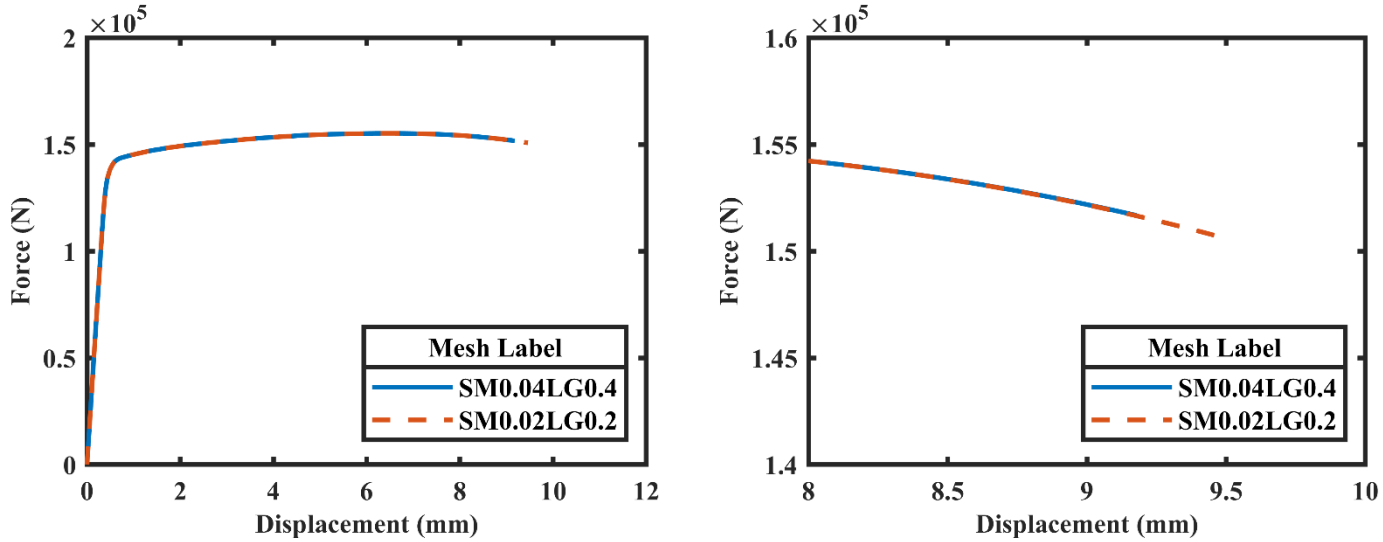


a) Mesh refinement with AWG regularization, 10x scaled geometry

b) Zoomed in on the failure portion of the curves shown in part a)

Figure 8: Refinement study for the 10x scaled geometry with AWG mesh regularization

Mesh regularization by scaling the failure criterion is not successful in reducing mesh dependence for the 10x (large) geometry, in fact the results using mesh regularization at the 10x geometry have worse agreement than the results without regularization with the same meshes. This may seem surprising, since the AWG regularization was created specifically to get meshes to match 0.2 mm size element results, especially under quasi-static uniaxial tension.

The 10x scale (large) geometry results converged to 9.46 mm displacement to failure without regularization, making little regularization required to match the 0.2 mm sized elements of mesh SM0.02LG0.2 in Table 5. The mesh SM0.04LG0.4 is still quite refined and has elements of about 0.4 mm in the 10x (large geometry). A mesh for the unscaled (small) geometry with elements approximately 0.4 mm in size (the mesh SM0.4LG4.0) is coarse. The stress gradient in a small geometry like the unscaled tensile specimen will be far greater than that in the analogous 10x scaled large geometry. For the large geometry, elements of approximately 0.4 mm size are sufficient in capturing the stress field, but for the small geometry 0.4 mm size elements are too coarse to capture the stress field as well. Thus, the AWG regularization curve (which was created from the unscaled geometry) "over corrects" the displacement to failure in the 10x geometry, and results in the percent difference with the 0.2 mm, SM0.02LG0.3 result to be an order of magnitude larger than the analogous result without mesh regularization.

## Results: Creation of Mesh Regularization Curve with Different Geometries

In the previous section, regularization by scaling the failure criterion was shown to be more effective for some geometries than others, even with the stress state held constant. It can also be shown that the regularization curve used to scale the failure criterion may not be unique for a particular state of stress, which will be discussed in this section.

Only the meshes having elements of target size of 0.2 and 0.4 mm in size are considered for the creation of these new regularization procedures. The SM0.2LG2.0 and the SM0.4LG4.0 meshes were used for the unscaled (small) geometry, and the SM0.02LG0.2 and the SM0.04LG0.4 meshes were used for the 10x scaled (large) geometry.

This resulted in a mesh of (roughly) 0.2 and 0.4 mm size elements for both geometries, but with the key difference being that the meshes for the unscaled (small) geometry are somewhat coarse, while the meshes for the 10x scaled (large) geometry are quite refined. The exact element sizes for these meshes can be found in Table 1.

Here we will follow what was done for the AWG model [6], which was to use mesh regularization to get the 0.4 mm mesh to match the displacement to failure found in the 0.2 mm mesh. The regularization used in MAT_224 indirectly influences the displacement to failure by scaling the failure criterion according to element size (there is also an ability to define a stress state dependence on the scale factor [2], but this work is using uniaxial tension. The value of the regularization scale factor to get the displacement to failure in the 0.4 mm mesh to match that of the 0.2 mm mesh was found by a trial and error process.

As shown in the previous results section, displacement to failure converges with mesh refinement for the uniaxial, plane-stress tension simulations of this work without the use of mesh regularization. Because of this, the dense meshes used in the 10x scaled (large) geometry need very little influence from mesh regularization to match, while the somewhat coarse meshes used in the unscaled (small) geometry require much stronger regularization to match the displacement to failure. The results of the regularization curve are summarized in Table 7.

Table 7: The regularization scale factors for the meshes of roughly 0.4 mm sized elements, calculated in both the unscaled (small) and 10x scaled (large) geometry. The unscaled case in this table was scaling to the SM0.2LG2.0 mesh, while the 10x scaled was scaling to match the corresponding simulation with mesh SM0.02LG0.2.

| Geometry | Mesh Label | Regularization Scale Factor | % Difference from corresponding result with elements of approx. 0.2 mm size |
|---|---|---|---|
| Unscaled | SM0.4LG4.0 | 0.846 | 15.4 |
| 10x Scaled | SM0.04LG0.4 | 0.996 | 0.4 |

As seen in Table 7, the geometry used has a strong influence over the resulting regularization curve's scale factors. Since the size of the elements were roughly the same in both the unscaled and 10x scaled geometries, the 10x scaled geometry had far more elements, and thus a refined mesh, while the unscaled geometry had a relatively coarse mesh. The tension simulations resulted in a regularization scale factor on the 10x scaled (large) geometry that is nearly unity. However, since elements (of similar size) on the smaller geometry give a coarse mesh, the regularization scale factor on the unscaled geometry is much more significant. This difference in scale factor is shown as the vertical axis in Fig. 9.

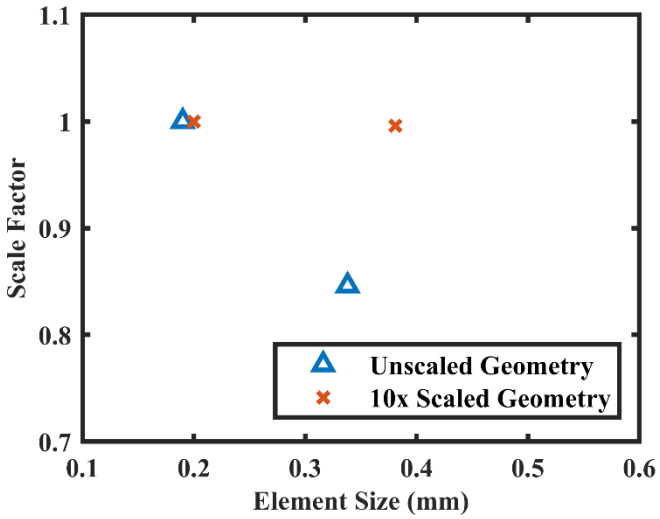


Figure 9: Regularization curves are strongly dependent on the geometry used to create them. See Table 1 for element sizes.

## Conclusions

Several aspects of mesh regularization with MAT_224 were considered to provide guidance on the application of the Ti-6Al-4V model available by the LS-DYNA Aerospace Working Group for use in future studies. That material model comes with a mesh regularization curve intended for elements ranging in size from 0.1 to 0.4 mm and scales the failure criterion for each element according to its size. In this work, it was shown that extending that preexisting regularization curve is not possible. To do so would require running larger geometries in order to determine regularization scale factors for larger element sizes. It was shown that the regularization scale factors inherently depend on the geometry used to calculate them, so a consistent regularization curve across geometries could not be made.

A refinement study of simulations on a quasi-static, plane stress, uniaxial tension test showed convergence without mesh regularization. Simulations with the unscaled geometry showed that the mesh regularization used in this work can improve agreement of results across different meshes for some conditions. Those conditions were that the stress state, element sizes, and geometry all be consistent with those that were used to create the regularization curve. However, the mesh regularization considered in this work also has the potential to overfit the model and thus increase mesh dependence and reduce accuracy when the geometry or stress state are not consistent with how the regularization curve was created, which was the case for the 10x scaled (large) geometry.

The mesh regularization used in this work, scaling the element failure criterion according to element size, would work well when the same geometry and stress state are used for both the calculation of the regularization curve and all other analyses. A common example of when this regularization would be useful is for models of fasteners, where in a full-scale simulation there may be thousands of fasteners where fully converged meshes are prohibitively expensive. This work also shows that running without mesh regularization in the MAT_224 Aerospace Working Group model gave satisfactory agreement to experimental tension results while avoiding the overfitting that can occur in regularized models.

## Appendix: Verification of the Use of the Symmetric Boundary Conditions

A comparison between the 1/8 symmetry and the full geometry models was made to validate the use of symmetric boundary conditions in this work. The full (not using symmetry boundary conditions) geometry was made by copying, rotating, and merging nodes from the symmetry model's mesh to create the full tensile specimen. The results of the comparison of the models of a simulated tensile test are given in Fig. 10. Since the results match quite well, the 1/8 symmetry model was used for the rest of the analysis.

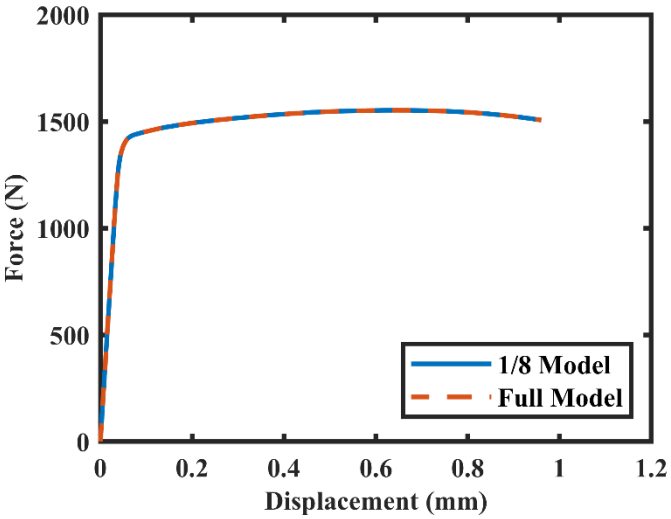


a) The 1/8 symmetry and full models

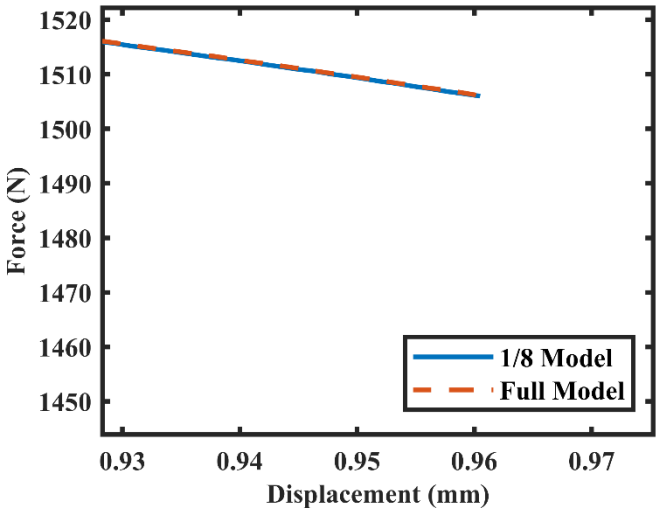


b) The 1/8 symmetry and full models zoomed in on the failure region

Figure 10: The force vs. displacement measured from the full and 1/8 symmetry models

### Acknowledgements

The authors would like to thank Eric Kurstak, Dino Celli, and Dushyanth Sirivolu for their support with revisions while writing this paper.

## References

[1] Belytschko, T., Bazant, Z. P., Yul-Woong, H., and Ta-Peng, C., 1986. “Strain-softening materials and finite-element solutions". Computers & Structures, 23(2).
[2] Pijaudier-Cabot, G., and Bazant, Z. P., 1987. “Nonlocal damage theory". Journal of Engineering Mechanics, 113(10), pp. 1512{1533.
[3] Livermore Software Technology Corporation, 2020. LS-DYNA Keyword User's Manual: Volume 2.
[4] Schwer, L. E., 2010. “A brief look at MAT NONLOCAL: A possible cure for erosion illness?". In 11th International LS-DYNA Users Conference.
[5] Hadjioannou, M., Stevens, D., and Barsotti, M., 2016. “Development and validation of bolted connection modeling in LS-DYNA for large vehicle models". In 14th International LS-DYNA Users Conference.
[6] Haight, S., Wang, L., Du Bois, P., Carney, K., and Kan, C.-D., 2016. “Development of a titanium alloy Ti-6Al-4V material model used in LS-DYNA. Tech. rep., George Mason University, The George Washington University, NASA Glenn Research Center.
[7] Johnson, G. R., and Cook, W. H., 1985. “Fracture characteristics of three metals subjected to various strains, strain rates, temperatures and pressures". Engineering Fracture Mechanics, 21(1), pp. 31 {48}.
[8] Buyuk, M., 2013. “Development of a tabulated thermo-viscoplastic material model with regularized failure for dynamic ductile failure prediction of structures under impact loading". PhD thesis, The George Washington University.
[9] Seidt, J., 2010. “Plastic deformation and ductile fracture of 2024-t351 aluminum under various loading conditions". PhD thesis, The Ohio State University.
[10] LS-DYNA Aerospace Working Group Website. https://awg.lstc.com/tiki-index.php.
[11] Lyons, T., and D'Souza, K., 2019. “Parametric study of a unmanned aerial vehicle ingestion into a business jet size fan assembly model". Journal of Engineering for Gas Turbines and Power, 141(7).
[12] Hammer, J. T., 2012. “Plastic deformation and ductile fracture of Ti-6Al-4V under various loading conditions". Master's thesis, The Ohio State University.
[13] Flanagan, D., and Belytschko, T., 1981. “A uniform strain hexahedron and quadrilateral with orthogonal hourglass control". International Journal For Numerical Methods In Engineering, 17(5), pp. 679{706}.
[14] LS-DYNA Aerospace Working Group MAT 224 User Guide, 2020. https://awg.lstc.com/tiki-index.php.